RMetS
Royal Meteorological Society

Attribution of strong winds to a cold conveyor belt and sting jet

D. J. Smart[a]* and K. A. Browning[b]
[a]*University College London, UK*
[b]*Independent researcher, Ambleside, UK*

*Correspondence to: D. J. Smart, Aon Benfield UCL Hazard Centre, University College London, 136 Gower Street, London WC1E 6BT, UK. E-mail: d.smart@ucl.ac.uk

A high-resolution version of the WRF (Weather Research and Forecasting) model has been used to study the fine structure of a cloud head and its associated cold conveyor belt jet (CJ) and sting jet (SJ) in an intense extratropical cyclone that produced damaging surface winds in northern Ireland and central Scotland on 3 January 2012. The model was run with many different initialisation times and physical parametrisations, and a run was selected that verified well against a variety of observations. New methods have been devised to visualise the 3D structure of the CJ and SJ and to attribute strong surface winds to one or other of them, and the validity of regarding the SJ as a semi-Lagrangian feature has been assessed. The model suggests that, whereas the CJ remained mainly below the 850 hPa level as it circulated around the bent-back front, the SJ consisted of a stream or streams of air within the bent-back frontal zone that first ascended from close to the surface into the middle and upper-level parts of the cloud head before descending from evaporating cloud filaments at the tip of the cloud head and reaching the top of the boundary layer slightly ahead of the CJ. The simulations did not support the idea that either the evaporation or conditional symmetric instability (CSI) played a major role in the development of these jets. The strong gusts (up to 47 m s^{-1}) which were recorded on the north coast of Ireland appear to have been due mainly to the CJ, which by then was undercutting the SJ. The SJ was responsible for stronger surface winds than the CJ several hours earlier during the initial stage of frontal fracture, but only for a limited period.

Key Words: extratropical cyclone; damaging winds; frontal fracture; bent-back front; WRF; mesoscale model

Received 22 October 2012; Revised 22 February 2013; Accepted 27 March 2013; Published online in Wiley Online Library 12 June 2013

Citation: Smart DJ, Browning KA. 2014. Attribution of strong winds to a cold conveyor belt and sting jet. *Q. J. R. Meteorol. Soc.* **140**: 595–610. DOI:10.1002/qj.2162

1. Introduction

It has long been recognised that there is a certain kind of extratropical cyclone that is liable to produce the most damaging winds. This is a cyclone that goes through a process of frontal fracture leading to the formation of a bent-back front (BBF; Shapiro and Keyser, 1990; Neimann *et al.*, 1993). Norwegian meteorologists were the first to realise that the strongest winds tend to occur in association with the BBF which they referred to as 'the poisonous tail' (Grønås, 1995). The winds there tend to reach their peak when the cyclone is close to attaining its lowest central pressure. This often follows a period of sustained and rapid development: deepening by 24 hPa or more in 24 hours may occur. A cyclone undergoing such explosive development is referred to as a meteorological 'bomb' by Sanders and Gyakum (1980). The synoptic evolution of one such storm which produced extreme wind damage in northwest France and southeast England in October 1987 was studied by Shutts (1990). He showed that the cyclone centre was associated with an upper-level potential vorticity (PV) maximum on the northern boundary of a very strong westsouthwesterly

airstream with an upper-level jet streak reaching almost 90 m s^{-1} at 250 hPa. At the surface the cyclone centre was associated with a wave in the thermal field, causing local enhancements of the very intense thermal gradients in the region where the BBF formed.

There are two kinds of jet-like features that give rise to the strong surface winds associated with the BBF. One is associated with the cold conveyor belt (Carlson, 1980; Schultz, 2001). It takes the form of a low-level jet, centred below 800 hPa, situated on the cold side of, and close to, the sharp surface front of the BBF. Forming part of the cold-frontal circulation, we refer to this jet as the cold-conveyor-belt jet, or CJ. The other potential source of strong surface winds is the sting jet (SJ), identified by Browning (2004) from an observational mesoanalysis of the extreme windstorm of October 1987. According to that study, the SJ produces strong winds that reach the surface in the dry air just ahead of the tip of the hook-shaped cloud head that accompanies the BBF. We must, of course, not lose sight of the fact that the overall severity of a cyclone is primarily determined by the interaction of the over-running potential vorticity anomaly with the underlying baroclinic zone and that the SJ is merely a secondary factor in creating a further, local, intensification of the wind.

Both CJs and SJs can produce strong winds but Browning (2004) suggested that SJs have the potential sometimes to produce slightly stronger winds and that, in situations of the kind being discussed here, with surface gusts reaching >40 m s^{-1}, a further, even small, increase in wind speed can have a disproportionate impact on the degree of damage produced. A recent study by Martinez-Alvarado *et al.* (2012) has shown that up to a third of the hundred most intense North-Atlantic winter windstorms over the last two decades have satisfied conditions for SJs. Since SJs may be a more common event than has hitherto been suspected, it is important to shed more light on their ability to generate strong winds which actually penetrate to the surface with the potential to create more damage than the better-known CJs.

Browning (2004) argued that the SJ occurred within air that had recently undergone cooling by evaporation of cloud and precipitation and suggested that this might play a significant role in the generation of the strong winds. The existence of rapid evaporation was consistent with the observation that the wind speed at this location greatly exceeded the rate of advance of the tip of the cloud head from which the SJ air was emanating. A follow-up study of the October 1987 storm (Clark *et al.*, 2005), using the Met Office Unified Model (UM), supported the idea of a SJ with a significant degree of evaporative cooling: the SJ air was shown to have originated in the cloud head at mid-levels and the potential temperature (θ) of some of the SJ air decreased as it descended on surfaces of constant wet-bulb potential temperature (θ_w). Significantly, these θ_w surfaces were *within* the frontal zone of the BBF rather than in the cold air as in the case of the CJ. This, together with its descent, is an important criterion for distinguishing between a SJ and a CJ. At the same time, it also indicates one of the potential difficulties in accounting for strong surface winds in terms of a SJ: the higher θ_w of the SJ, together with its adiabatic warming during descent which is only partly compensated by latent cooling, results in an increase in static stability. Thus the downward transfer of momentum to the surface is inhibited unless the degree of latent cooling is sufficient to enable either shearing instability or convective instability to occur. In the absence of these processes, the extent to which internal gravity waves produce downward transfer of momentum is an open question. Convective overturning did occur in parts of the October 1987 storm (Browning, 2004; Browning and Field, 2004) but evidence was lacking to prove that it was occurring extensively throughout the entire region thought to have been affected by strong surface winds from the SJ.

The first direct observational evidence for the existence of a SJ aloft was obtained by Parton *et al.* (2009) when the tip of a cloud head passed over a wind-profiler radar. They observed shallow convective clouds in the lowest 2 km just ahead of the tip of the cloud head and suggested that this was an example where convection was able to transfer momentum from the SJ to the surface. Although Parton *et al.* (2009) found that the UM was able to reproduce the SJ in their case, they found that it failed to reproduce the convection that is thought to have brought the associated strong winds to the surface. This may be because the UM tends to underestimate the degree of evaporational cooling in the SJ. Martinez-Alvarado *et al.* (2010), in a case-study of another SJ, found that the COSMO (COnsortium for Small-scale MOdelling) model gave significantly more evaporational cooling than the UM.

When using either satellite imagery or weather radars to detect the cloud heads within which these jets form, a typical feature to be observed is bandedness in the cloud and precipitation, orientated parallel to the BBF. Dropsonde measurements across a cloud head by Browning *et al.* (1995) showed that these bands were associated with slantwise layering in both thermodynamic and kinematic fields within the cloud head. The structure of cloud heads is in many respects similar to that within ana-cold frontal cloud systems in general, and a study of stacked slantwise convective circulations observed in such a system led Browning *et al.* (2001) to suggest that these circulations might be enhanced by conditional symmetric instability (CSI). In the study of the October 1987 storm, Browning (2004) (his Figure 14) envisaged a scenario in which multiple slantwise circulations, perhaps enhanced by CSI, might create multiple SJs. Although CSI theory is strictly valid only for purely 2D flows, the recent modelling studies by Martinez-Alvarado *et al.* (2010) and Gray *et al.* (2011) have provided strong evidence for a possible role of CSI in the development of a SJ forming within a cloud head.

On 3 January 2012 an intense cyclone ('bomb'), of the kind discussed above but not as intense as the October 1987 storm, produced a swath of damaging winds extending from northern Ireland across to the Central Lowlands of Scotland. As shown by the infra-red satellite imagery in Figure 1, the storm produced a classic cloud head with multiple-banded structure. Figures 1(a) and (b) show the evaporating tips of these cloud bands, or filaments, passing close to the north coast of Ireland at times when strong winds were occurring there. The lines a, b, c and d, representing four of the filaments in Figure 1, were derived subjectively (by manually tracing METEOSAT satellite imagery) but, at least over the period spanning the times of Figures 1(a) and (b), their continuity was unambiguous when viewing a sequence of images at 15 min intervals. A peak gust of 47 m s^{-1} occurred at 0536 UTC at Malin Head near the tip of filament 'c' in Figure 1(b). In the present article, we use an observationally validated high-resolution run from

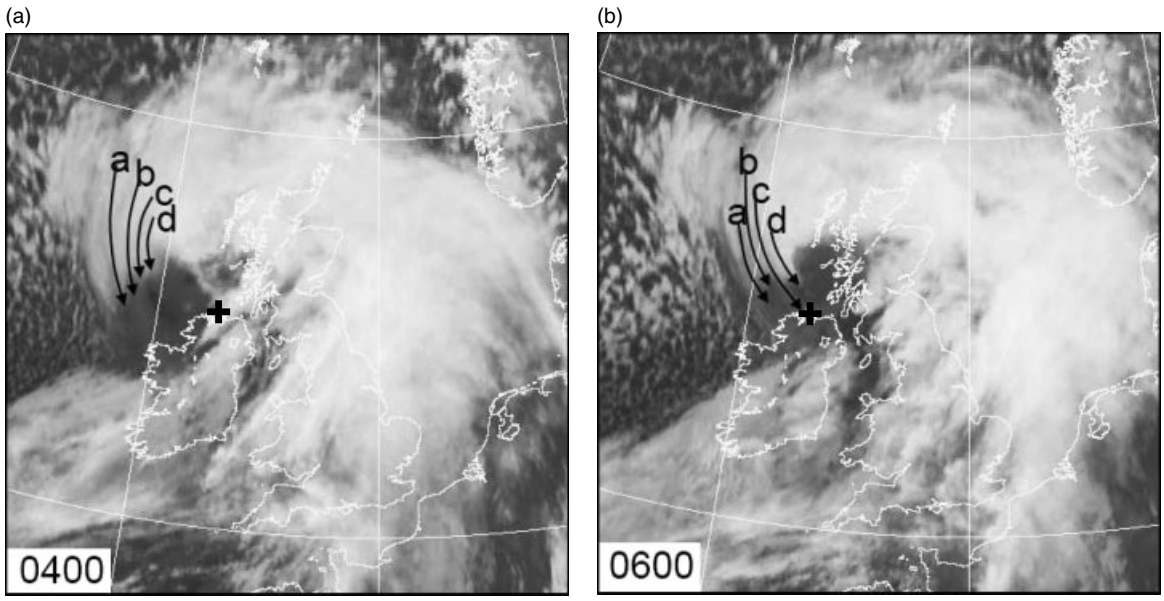

Figure 1. MSG (MeteoSat Geostationary) IR imagery at (a) 0400 UTC, (b) 0600 UTC on 3 January 2012. Four cloud filaments a, b, c, d are indicated by the labelled arrows (derived from examination of 15 min imagery). (Courtesy and copyright EUMETSAT/UKMO). The location of Malin Head is marked by a +.

the WRF (Weather Research and Forecasting) model to investigate the evolving 3D structure of the CJ and SJ in this storm, and thereby clarify their relationship to one another and, as far as possible (given the possible limitations of the model in, for example, representing the effects of latent cooling), determine which kind of jets were likely to have been responsible for the strongest surface winds during and before the period when it was affecting the north of Ireland. This period was chosen because it included some of the strongest surface winds and because much of the system was over the sea and relatively uninfluenced by topographical effects which did not appear to be well represented by the model.

The article is structured as follows. In section 2, the configuration of the WRF model is described, together with the reasons for selecting a particular run, initialised as much as 3 days before the storm arrived. In section 3, the chosen run is evaluated against a variety of observational sources. We believe that the credibility of our study owes a lot to the painstaking validation of the model against observations and the selection of the best performing model run from a variety of runs not only initialised at different times but also using different combinations of parametrisation schemes. Model diagnostics showing the 3D structure of the jets are given in section 4.1 for a time during the mature frontal fracture phase of the storm before it made landfall. The evolution of the footprint of strong surface winds and their attribution to the CJ and SJ are presented in section 4.2. A general discussion and conclusions are given in section 5.

2. The model

The version of WRF used in this study was the Advanced Research WRF (ARW-WRF) 3.2.1 (Skamarock *et al.*, 2008). A one-way nested configuration was employed whereby the initialisation data were first interpolated to a large domain ('Domain 1') with 15 km grid spacing on a Lambert conformal grid, covering much of the the North Atlantic and Northwest Europe region (421×371 horizontal grid points, centred on 55°N, 25°W). Hourly output from this domain was then used as initial and boundary conditions for a 5 km domain ('Domain 2') (501×461 horizontal grid points, centred on 52.5°N, 10°W). The vertical grid had 48 levels with a stretching function to give spacing of 120–240 m in the lower and mid-troposphere, with the lowest, full model level at 24 m above the terrain and the model top at 50 hPa. Although the number of levels here is less than that employed in the studies by Clark *et al.* (2005) and Martinez-Alvarado *et al.* (2010), no significant difference could be found in the intensity and structure of the modelled jets when compared to a run having 90 default WRF levels (spacing of ∼140–280 m in the lower and mid-troposphere, model top at 50 hPa) . The initialisation data were obtained from the NCEP (National Centers for Environmental Prediction) GFS (Global Forecast System) model. Additionally, high-resolution (1/12° NCEP sea surface temperature (SST)) data were incorporated into the initialisation data. Both domains were initialised at 1200 UTC on 2 January 2012 and run for 24 h. Full history files from Domain 2 were saved every 15 min and a sub-set of data every 5 min.

Simulations initialised from various GFS operational runs from 1–2 days prior to 3 January were found to produce a storm insufficiently deep (960 hPa) compared to observations and compared with the UKMO (United Kingdom Meteorological Office) analysis of 952 hPa at 0600 UTC on 3 January (Figure 2(a)), although the track was generally good, thus providing useful guidance for forecasters. A run initialised with GFS FNL (Final Analysis) data produced similar results. However, by inspecting runs initialised up to three days earlier, a run was found which verified well in terms of track and intensity although 1.0–1.5 h late. This was the GFS operational run initialised at 0600 UTC on 31 December 2011 and data from this run, starting at 1200 UTC on 2 January 2012 (T+54 h), were employed in all the simulations reported here.

Different microphysical and boundary-layer parametrisations were employed in order to obtain the best comparison with available observations and these will be discussed

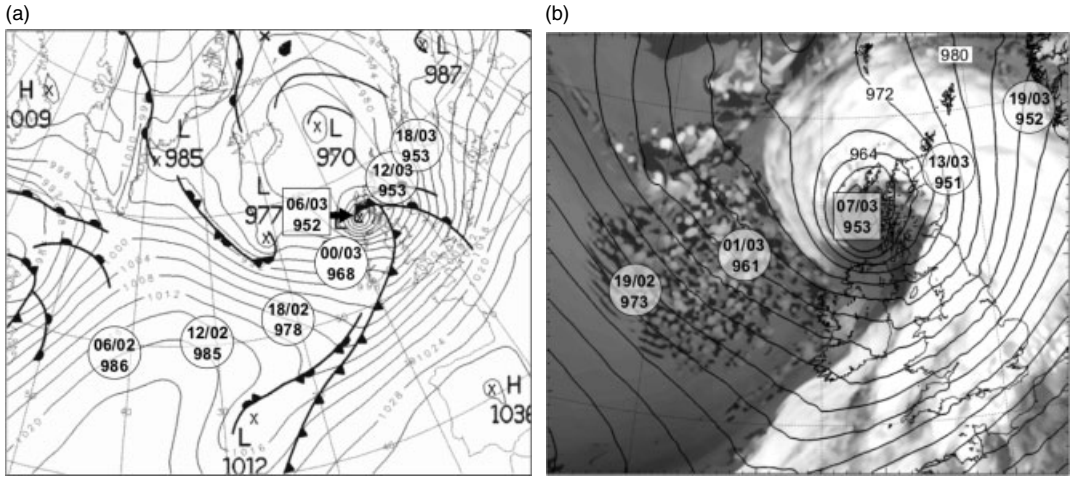

Figure 2. Comparison of surface analysis with model fields: (a) surface analysis at 0600 UTC on 3 January 2012 (by courtesy of and copyright UKMO), and (b) sub-area of model Domain 2 at 0700 UTC, with OLR shaded. In both frames, MSLP (hPa) is contoured every 4 hPa, the location of the model storm centre is indicated within the square box by time (UTC)/day/central pressure (hPa), and locations of the storm centre at other times are indicated by overlaid circles. Apparent differences in the track of the low centre in (a) and (b) are mainly due to differences in the orientation and scale of the projections.

further in section 3. However, the simulations were found to be relatively insensitive to deep and shallow cumulus parametrisation, boundary-layer vertical resolution and radiation parametrisation. For all simulations reported here the Kain–Fritsch (KF) cumulus scheme was employed on Domain 1, but not on the higher resolution Domain 2, and the Dudhia short-wave and RRTM (Rapid Radiative Transfer Model) long-wave radiation schemes were used on both domains. The reader is referred to Skamarock *et al.* (2008) for further details and references on the WRF parametrisation schemes.

Wind gusts at 10 m were diagnosed in post-processing using a computation based on the method of Schulz developed for the COSMO model (Schulz, 2008; Born *et al.*, 2012) and adapted for WRF.

3. The observations and model validation

In this section we outline results from simulations with differing parametrisations, all initialised at 0600 UTC on 31 December 2011, in which we use differing parametrisations and we then compare these with observations. Figure 2(a) shows the UKMO surface analysis for 0600 UTC on 3 January. Overlaid are the position and central sea-level pressure (SLP) of the storm at 6 h intervals prior to, and after, this time. The chart shows an intense low pressure system located just northwest of Ireland with a minimum central pressure of 952 hPa, having deepened 34 hPa in the previous 24 h. Figure 2(b) shows the outgoing long-wave radiation (OLR) and SLP fields from a sub-section of Domain 2 from a model run, as described in section 2, at a time in the run (0700 UTC) comparable to the 0600 UTC analysis. The minimum SLP from the model is overlaid at 6 h intervals. Although differences in terms of the evolution of the SLP centre are apparent, the central SLP at 0700 UTC (model time) is within 1 hPa of the analysis and the configuration of the high cloud, as depicted in the OLR field, compares favourably with satellite imagery (Figure 1(b)). In order to assess further the performance of the model, we compared 5 min output data with available surface observations from across Ireland and Scotland and especially the record from the Malin Head station (55.38°N, 7.37°W) (location marked in Figure 1). We focus on Malin Head because of its exposed coastal situation; wind gusts there peaked at 91 kt (47 m s^{-1}) at 0536 UTC and the mean wind speed attained 71 kt (36 m s^{-1}) at 0601 UTC (the peak mean wind speed is a provisional record for the station at time of writing). Figure 3 directly compares 5 min data (adjusted by 1 h) from the best performing run with the observations from Malin Head. In general the model reproduces the passage of the strongest winds well, although the mean magnitude of the model wind gusts is a few m s^{-1} too high and mean 10 m wind speeds too low. Particularly noteworthy is the marked drop in temperature, magnitude 4 °C, after 0400 UTC and prior to the onset of the strongest winds. Before the arrival of the strong surface winds, there was a shallow layer of warm air close to the relatively warm sea surface (SSTs northwest of Ireland were 10 °C according to the NCEP analysis – not shown). Thus the observed cooling of the surface air required the mixing down of cool air from above. The ability of the model parametrisation scheme to reproduce not only the strength of the surface winds but also this cooling, was used to determine which of the many runs performed was selected for detailed analysis.

The results from the ensemble of simulations are shown in Table 1. For this ensemble the model configuration was kept constant, as outlined in section 2, but the choice of microphysics (MP), planetary boundary-layer (PBL) and surface layer (SL) schemes was varied in a systematic manner. As the track and minimum SLP centre of the storm were within tens of km and 1–2 hPa of the observations for all members of this ensemble, we tabulate only differences in cooling, maximum mean 10 m wind speed and maximum 10 m wind gust at the closest grid point in Domain 2 to the location of Malin Head. Below we summarise some key points:

- The MYNN3 and MYNN2 (Mellor–Yamada–Nakanishi–Niino) schemes provided greater cooling than MYJ (Mellor–Yamada–Jancic), probably because they employ enhanced vertical mixing (Nakanishi and Niino, 2004).
- The prognostic turbulent kinetic energy (TKE) schemes MYJ, MYNN2 and MYNN3 in general

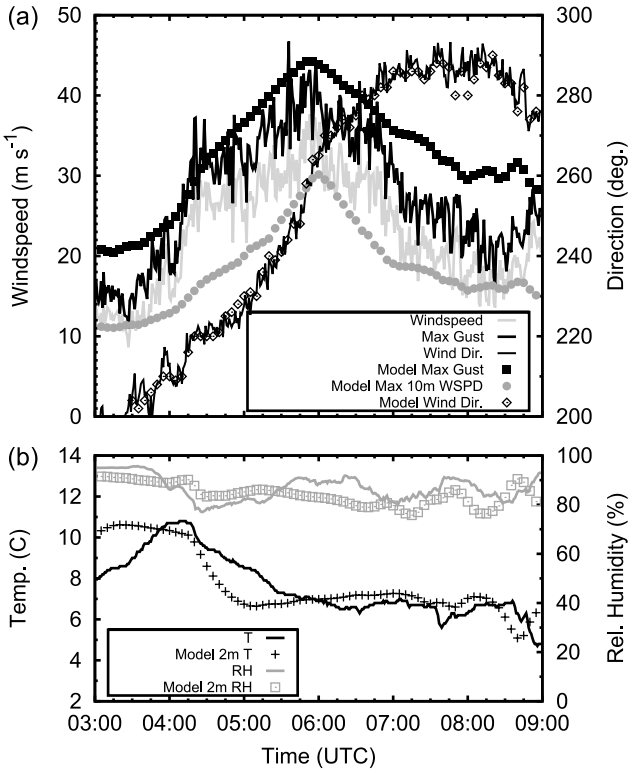

Figure 3. Comparison of model 5 min output for the WSM6/MYNN2/MYNN3 run (R01) with observations from Malin Head. (a) Surface mean wind speed, wind direction and wind gusts. (b) Surface temperature and relative humidity. The model data have been adjusted by −1 h to achieve a best fit with the observations. No spatial adjustment was required. (Malin Head data were kindly provided by Met Éireann).

outperformed the non-local YSU (Yonsei State University) scheme which, although it provided moderate cooling, was at least 1 °C too warm overall (not shown).

- The WSM6 (WRF single-moment 6) microphysics scheme outperformed other schemes in terms of cooling and maximum wind gusts, possibly because of the enhanced treatment of ice physics. However, the two-moment Thompson and Morrison schemes, despite their more sophisticated treatment of ice, performed relatively poorly in terms of cooling. Surprisingly the WSM3 (WRF single-moment 3), with only a simple treatment of ice physics, produced moderate cooling (3.3 °C).
- The WSM6/MYNN2/MYNN3 combination provided the most realistic cooling and gust velocities of all and was therefore adopted as the version used in deriving Figure 2(b) and all subsequent figures.
- All combinations significantly underestimated the peak 10 m mean wind speed.
- Although the WSM5 (WRF single-moment 5) and WSM6 (WSM5 including a treatment of graupel) microphysics schemes performed similarly in most respects, subjective examination of model relative humidity fields suggested WSM6 produced more clearly defined cloud head filaments (section 4.1) and the latter scheme was preferred.

We selected the WSM6/MYNN2/MYNN3 physics run (R01) for further detailed analysis. The model-diagnosed gusts for the R01 run are compared with observations from all available surface stations in Figure 4. The model reproduces the general gust 'footprint' quite well; however gust speeds inland are clearly too low. Examination of data from other runs with different physics combinations (not shown) shows this is a characteristic feature of the MYNN3 SL scheme (as implemented in WRF version 3.2.1) for this case. The MYNN2, MOJ (Monin–Obhukov–Jancic) and MO (Monin–Obhukov) SL schemes produced higher gusts inland but did not perform as well as MYNN3 in terms of reproducing the cooling at Malin Head.

4. Model diagnostics of the 3D structure

In this section we examine the chosen R01 run in detail. Our aim is to determine how the CJ and SJ develop and evolve prior to landfall along the coast of northern Ireland. In section 4.1 we analyse the model storm at 0300 UTC (i.e. a model time roughly comparable to 0200 UTC). Hereafter, all times refer to the model time, unless stated otherwise. We then describe the overall evolution of the flows prior to 0700 UTC in section 4.2.

4.1. 3D structure at 0300 UTC

We now analyse the structure of the model storm at model time 0300 UTC on 3 January. This time was selected

Table 1. Results of runs with different combinations of parametrisations (definitions are given in the text), compared with observations of surface wind speed and temperature drop associated with the arrival of the jets.

Ref.	MP	PBL	SL	$-\Delta T$ (°C)	Maximum mean wind speed ($m\,s^{-1}$)	Maximum gust ($m\,s^{-1}$)
Obs.	–	–	–	**4.1**	**36.5**	**46.5**
R01	WSM6	MYNN2	MYNN3	3.9	30.0	44.1
R02	WSM6	MYNN3	MYNN3	3.7	29.9	43.9
R03	WSM6	MYNN2	MYNN2	3.5	29.8	43.8
R04	WSM5	MYNN2	MYNN3	3.5	29.6	43.5
R05	THOMPSON	MYNN2	MYNN3	2.8	29.9	42.2
R06	MORRISON	MYNN2	MYNN3	3.0	30.0	42.0
R07	WSM6	MYNN2	MOJ	3.6	29.5	43.7
R08	WSM6	MYJ	MOJ	1.8	25.2	43.5
R09	WSM5	MYJ	MOJ	2.5	31.0	43.0
R10	WSM3	MYJ	MOJ	3.3	29.5	41.9
R11	WSM5	YSU	MO	2.9	30.4	42.8

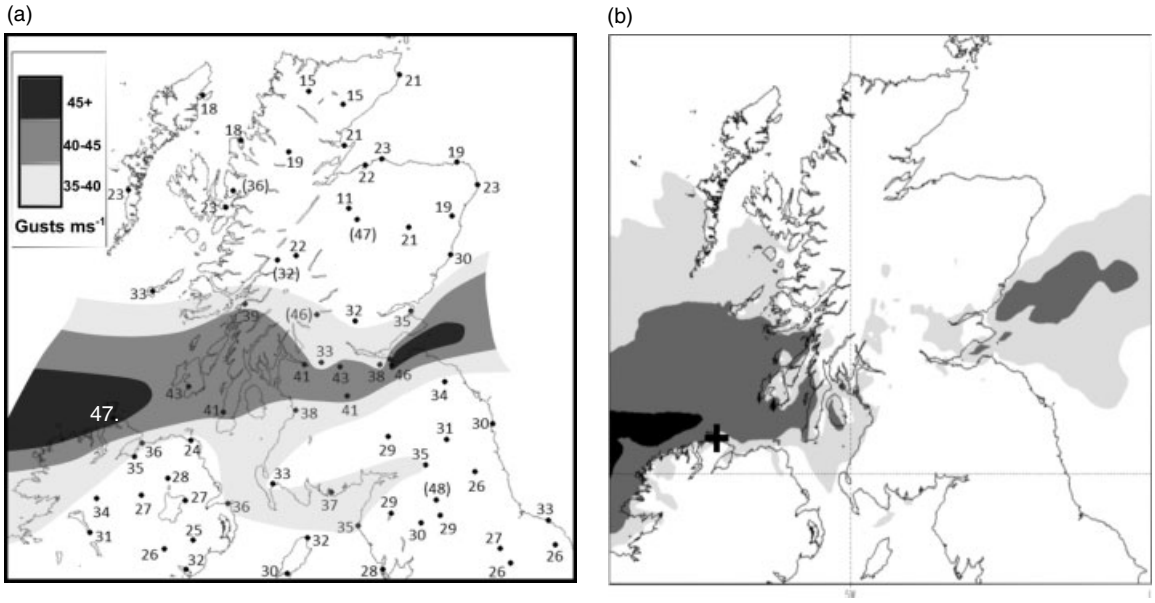

Figure 4. Comparison of time-integrated observed and modelled 10-m gust footprints. (a) Maximum surface gust observations ($m\,s^{-1}$) from weather stations, 0300–1200 UTC on 3 January 2012. Values from stations with elevations above 400 m are in brackets. The gust magnitude for Malin Head is shown in white. Manually interpolated gust contours, ignoring the bracketed values, are shaded according to inset key. (The original figure was kindly prepared by Matthew Clark from Met Office data, by courtesy of and copyright UKMO). (b) Time-integrated diagnosed maximum 10 m wind gusts ($m\,s^{-1}$), 0300–1200 UTC on 3 January (shaded as in (a)) from model Domain 2. The location of Malin Head is marked by a +.

because there are maxima in the surface wind gust footprint attributable to SJs which are distinct from the maximum due to the CJ at this time. We shall show evidence for a causal relationship between the individual jets and particular parts of the footprint of strong surface wind gusts. Figure 5 shows the structure of the BBF and frontal fracture regions at or close to the surface at 0300 UTC. We have labelled local wind speed maxima within the footprint of surface wind gusts according to whether they are shown to be due to the CJ or to one of two separate SJs: the sting jet labelled SJ2 corresponds, as we shall demonstrate, to the main SJ at this time and that labelled SJ1 corresponds to the remains of one that had been the main SJ at earlier times. Figure 5 shows that the two maxima labelled SJ1 and SJ2 are associated with θ_w values at 950 hPa, corresponding to a level only 200 m above the surface, of around 9.5 and 8.5 °C, respectively; the wind maximum labelled CJ is associated with a much lower value for θ_w of 6–7 °C.

In order to analyse the structure of the BBF and associated CJ and SJ, we have manually constructed a number of transverse sections along radials, at roughly 20° intervals, approximately normal to the BBF and radiating from the manually determined centroid of the arc formed by the BBF. This is a novel feature of the analysis which we consider necessary in order to deconstruct with confidence the various flows in the strongly curved environment of the BBF. Our experience of analysing this storm (and others) suggests this technique (as opposed to the Cartesian west–east/north–south sections used in previous SJ studies) provides a much clearer picture of these flows. Figure 6(a–f) shows six of these cross-sections: A–A′('A'), B–B′('B'), C–C′('C'), D–D′('D'), E–E′('E') and F–F′('F'). Two of the jets, CJ and SJ2, are identified in all six panels of Figure 6; the third jet, SJ1, is evident only in the final panel, section F.

The CJ, with a θ_w of 6–7 °C, is seen to be confined to the cold air beneath/behind the frontal zone (the θ_w for the CJ in Figure 5 is at the top end of the 6–7 °C range because Figure 5 is for a level close to the surface, towards which the

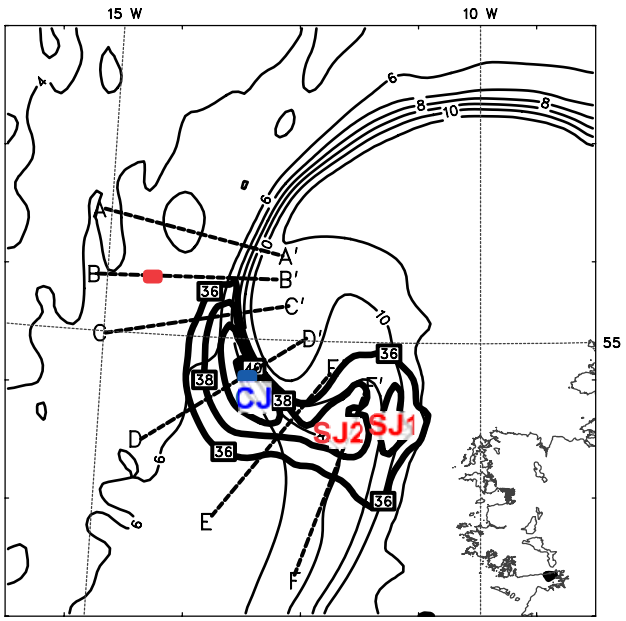

Figure 5. Model near-surface (950 hPa) θ_w field (°C; thin contours at 1 °C intervals) and diagnosed 10 m gusts ($m\,s^{-1}$; bold contours at 2 $m\,s^{-1}$ intervals from 36 to 42 $m\,s^{-1}$) at 0300 UTC on 3 January. The location of transverse cross-sections (A to F) are indicated by the dashed lines A–A′ to F–F′ (see text). The starting locations of the trajectories CJ and SJ shown in Figures 9 and 11 are within the small rectangular boxes on sections B–B′ and D–D′ respectively. Tick marks around the edge of the panel are at 100 km spacings. This figure is available in colour online at wileyonlinelibrary.com/journal/qj

temperature increases because of the warmer sea surface). The main SJ at this time, SJ2, with its θ_w between 8 and 8.5 °C, is embedded within the frontal zone. The jet SJ2 slopes down from transverse section to transverse section (i.e. at right angles to the sections): it is centred at 520 hPa in section A and descends to 750 hPa by section E, and 800 hPa in F. (This is not to say that individual air parcels necessarily

travel the full length of the jet axis, all the way from 520 to 800 hPa: they do not. As we shall see, trajectory analyses show that individual air parcels descend down only portions of the jet axis.)

The axis of the entire SJ2 starts from a position 70 km to the left (i.e. to the west) of the CJ in section A and reaches a position directly above the CJ between sections D and E. By the time the CJ reaches section E, the only evidence of the CJ is a weakening velocity maximum associated with air of slightly higher θ_w at its leading edge: the leading edge of the CJ air with θ_w of 6 °C lies somewhere between D and E. Finally, in section F, the CJ is seen to be totally absent and the dominant low-level jet, at 800 hPa, is SJ2 with a θ_w of 8 °C. The other sting jet, SJ1, can also be seen in section F: it has a slightly higher velocity than SJ2 but is higher up, with a higher θ_w of about 9 °C. As noted above and discussed later, SJ1 is responsible for the local maximum in the surface gust footprint labelled SJ1 in Figure 5, just ahead of the surface gust maximum due to SJ2. There is no evidence of SJ1 in any of the other sections in Figure 6(a–e), the portion of SJ1 in section F (Figure 6(f)) being just the remnant of the jet that had dominated during the preceding 3 h. We shall be focussing our attention mainly on SJ2 in this subsection.

To show the nature of the SJ more clearly, we employ the technique of analysing the model fields on moist isentropic surfaces (Figures 7(a, b)). The moist isentropic framework (e.g. Browning and Harrold, 1969) assumes that the flows are essentially confined to and conserved along moist isentropic (i.e. constant θ_w) surfaces assuming minimal mixing and essentially moist adiabatic processes. We demonstrate later that this is a good approximation for air parcels in the SJ. It is a poorer assumption for the CJ but the conclusions we draw from the corresponding analysis are thought to be broadly correct. Figure 7(a) gives the analysis for the 6 °C θ_w surface to represent the CJ (the axis of which is shown by the dashed arrow) and Figure 7(b) shows the corresponding analysis for the 8.5 °C surface to represent SJ2 (the bold, solid arrow). Figure 7(a) shows the CJ remaining within saturated or almost saturated air in the lower part of the cloud head with very little significant change of height in time, whereas the strongly sloping axis of SJ2 can be seen originating within the saturated air of the cloud head (white shading) and then emerging from it. The rate of advance of the leading edge of the cloud head is slower, by as much as 17 m s^{-1}, than the velocity of the air in SJ2, which is symptomatic of the ongoing evaporation of the tip of the cloud head in this region of descending flow. The descending air in SJ2 undergoes strong divergence as it nears the surface and this leads to the widening of the gap between the 8 and 9 °C θ_w contours at 950 hPa that was evident in Figure 5; this is, of course, all part of the process of frontal fracture.

Figure 8 summarises the disposition of the principal jets as analysed in Figures 5–7. Both the CJ and the SJ are seen to curve around the cloud head. The CJ remains centred close to 900 hPa whilst the SJ descends from 520 to 800 hPa. The two jets originate from different parts of the cloud head but, by the time they reach the position of section D, they are close together in plan view, almost one above the other in the region experiencing the strongest surface winds.

Diagnostics for sets of air parcel trajectories, initiated at 0300 UTC (15 h into the model run) along the axes of the CJ and SJ2, are shown in Figure 9. Trajectories were computed from 15 min history files and interpolated to 5 min intervals using the RIP (Read-Interpolate-Plot) 4 package (Stoelinga, 2009). The trajectories were initialised from around the core of each jet, i.e. the centre of the maximum closed isotach or the centroid of the jet maximum as determined by inspection of the relevant cross-section. The three curves shown for each jet in Figure 9 correspond to parcels initialised at 0300 UTC and ±5 km from the actual jet core. The CJ trajectories, (light grey in Figure 9), were started in the box in section D in Figure 5 and carried 6 h backwards and 3 h forwards from there. The trajectories for SJ2 were started in the box in section B; this particular starting position was selected because the resulting parcels exhibited relatively large vertical excursions. As will be shown shortly, parcels started at other locations along the axis of the SJ performed similarly apart from having smaller vertical excursions.

The properties of the SJ2 trajectories in Figure 9 are distinctly different from those of the CJ trajectories. For instance, the CJ parcels are not only cooler than the SJ2 parcels but are confined to levels below 850 hPa while maintaining a relatively constant humidity of 100%. The CJ parcels also change their θ_w significantly with time, especially after 0200 UTC when they warm rapidly, presumably because of mixing with air close to the warmer sea surface. The SJ2 parcels, on the other hand, retain a more consistent value of θ_w, thereby justifying the use of the moist isentropic analysis for SJ2 in Figure 7(b). What the CJ and SJ2 parcels have in common, however, is that they all attain wind speeds in excess of 45 m s^{-1} (although, at the surface, the winds due to the SJ are less intense than those due to the CJ because the SJ core does not penetrate to such a low level). Focussing now on the behaviour of the SJ2 trajectories in Figure 9, the key features are:

- a 3–5 h period of fairly rapid ascent (typically 20 cm s^{-1}) with cloud mixing ratio increasing to 0.1 g kg^{-1}, during which the (dry-bulb) potential temperature (θ) increases and the wind speed decreases to below 10 m s^{-1}, followed by –
- a 3–4 h period of fairly rapid descent (typically 20 cm s^{-1}) during which the (not very dense) cloud evaporates, relative humidity decreases from 100% to 20%, and the wind speed increases rapidly to over 45 m s^{-1}. However, the air parcels experienced negligible potential cooling due to evaporation (generally less than 1 °C), so presumably their rapid acceleration was due more to larger-scale dynamical processes as they circulated around the BBF.

The total descent of the SJ2 parcel exhibiting the greatest descent in Figure 9 is about 185 hPa (i.e. from about 520 to 705 hPa) which, though large, is less than the vertical extent of SJ2 at 0300 UTC: indeed, Figure 6 shows that the axis of SJ2 can be traced all the way from 800 to 520 hPa. In other words, these parcels do not follow the axis of SJ2 along its entire length.

An interesting question relates to the extent to which the SJ can be considered to be a semi-Lagrangian airstream in which at least some individual air parcels can descend along a substantial portion of the SJ as observed at a given time. To address this point, we have initiated trajectories at 0300 UTC at three locations in and around the SJ core as identified in each of the six cross-sections in Figure 6. Figure 10(a) shows plots of the mean pressure for each set of three trajectories for the parcels initiated in these six locations along the axis of the SJ. Some of these, in the upstream portion of the SJ, were initiated at high levels,

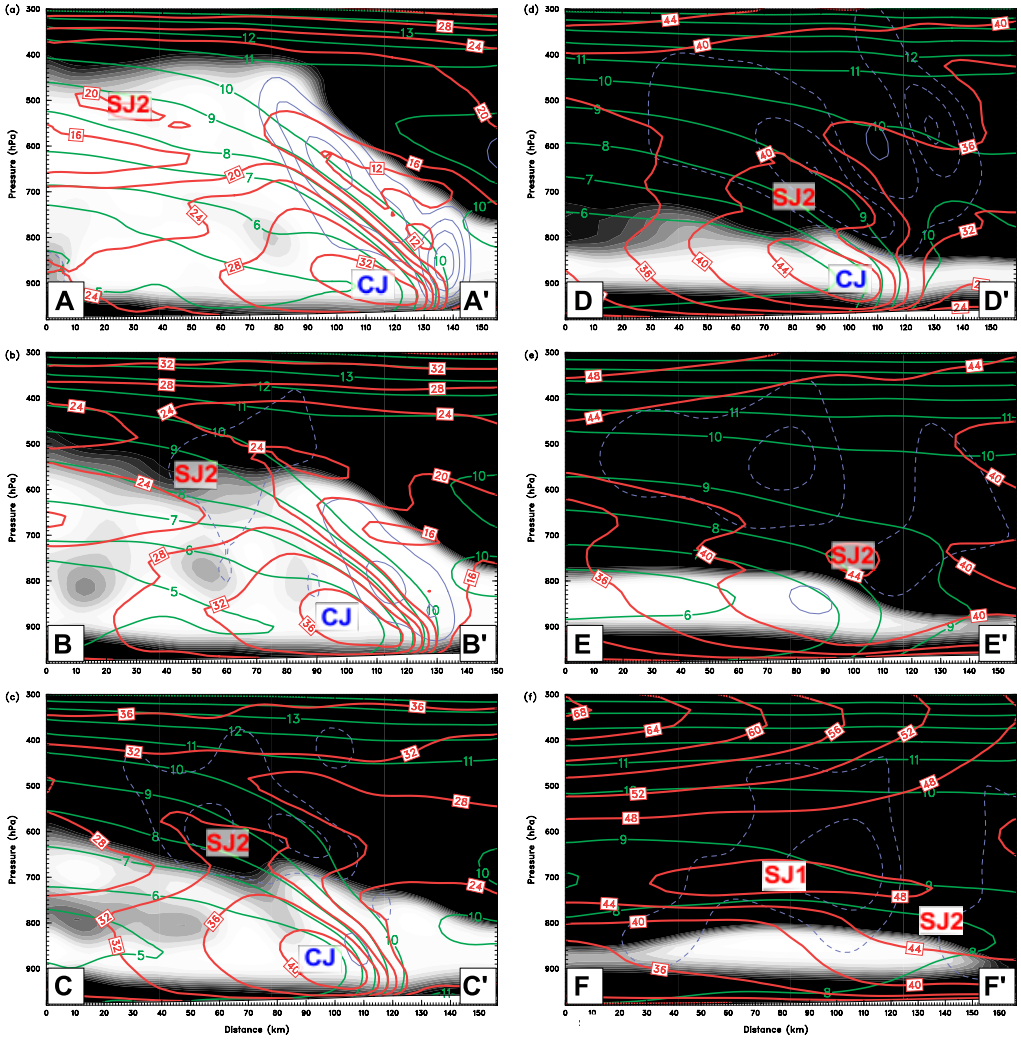

Figure 6. Cross-sections showing the vertical structure of the BBF at 0300 UTC on 3 January. (a, b, c, d, e, f: sections A–A′, B–B′, C–C′, D–D′, E–E′, F–F′. Figures 5 and 7 show locations.) Relative Humidity w.r.t. ice (RHi) (%), shaded from 90% (black) to 100% (white); θ_w (°C), medium contours every 1 °C; earth-relative horizontal wind speed (m s^{-1}), bold contours every 4 m s^{-1}; vertical velocity (cm s^{-1}), fine contours every 10 cm s^{-1}, with negative dashed and zero omitted. The locations of the main jet cores (see text) are annotated. This figure is available in colour online at wileyonlinelibrary.com/journal/qj

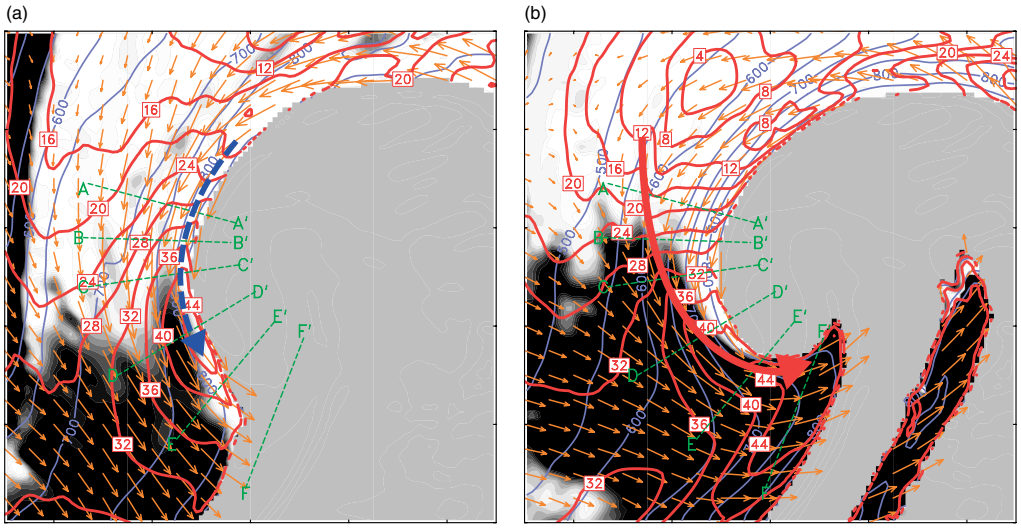

Figure 7. Moist isentropic analyses of the CJ and SJ at 0300 UTC on 3 January on (a) 6 °C θ_w surface and (b) 8.5 °C θ_w surface. RHi (%) is shaded from 90% (black) to 100% (white); earth-relative horizontal wind speed (m s^{-1}, bold contours every 4 m s^{-1}); pressure (hPa, fine contours every 50 hPa); system-relative wind vectors. For simplicity a system velocity of 17.9 m s^{-1} is assumed for both surfaces. The axes of the CJ (dashed arrow) and SJ (bold, solid arrow) are indicated. The locations of transverse sections are indicated by the dashed lines, labelled A–A′ to F–F′. Fields below the earth's surface are masked out. Boundary tick marks are every 100 km. This figure is available in colour online at wileyonlinelibrary.com/journal/qj

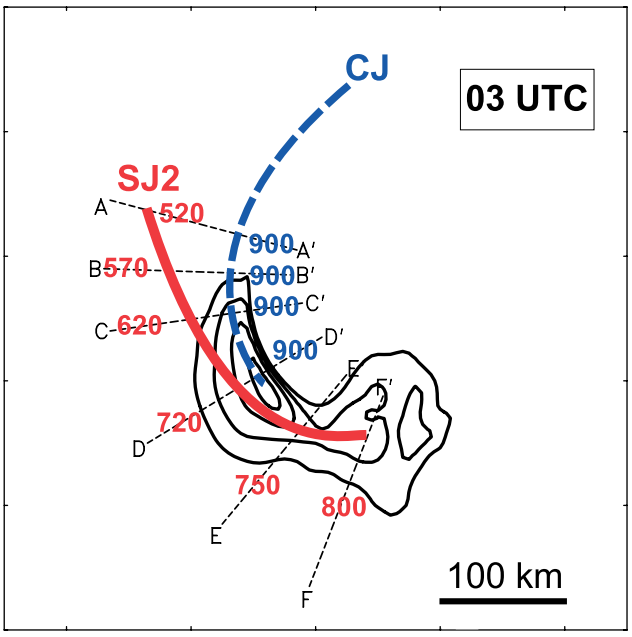

Figure 8. Partial schematic showing the principal jets at 0300 UTC on 3 January. The area covered is the same as in Figures 5 and 7. The axes of the CJ (dashed line) and SJ (solid, bold line) are shown, with the approximate pressure of the jet core annotated where the jets cross the transverse sections. Diagnosed 10 m wind gusts ($m\,s^{-1}$) appear as bold contours from 36 to 42 $m\,s^{-1}$. The transverse cross-sections are indicated by the dashed lines A–A′ to F–F′ (see text). This figure is available in colour online at wileyonlinelibrary.com/journal/qj

whilst others, in the downstream portion, were initiated at much lower levels. What all of these trajectories have in common is an early period of ascent followed by a period of descent lasting at least 3 h. Various properties of these parcels are given in Table 2 for the times when the descent began and ended; we also give the differences in the values over the period of descent. Here, and later in Figure 11, we give the values for the parcels that experienced the greatest vertical excursions rather than giving the means of three parcels as in Figure 10. For the moment, we focus just on the pressure. Parcels starting at all heights along the jet axis did indeed descend: the pressure increment is seen to be between 90 and 185 hPa. Thus the instantaneous representation of the SJ does indicate substantial descent along all parts of it; however, no parcels travel along its entire length which, as noted above, extends over a height interval corresponding to a pressure change of about 280 hPa. Table 2 shows that the descent takes place over a period of 2.75 h to as much as 4.50 h which is comparable with the lifetime of an individual SJ (see later), and this may be part of the explanation for parcels not descending along the entire length of the SJ. Therefore to regard the SJ as a semi-Lagrangian entity has to be treated as first-order approximation.

We drew attention above to the negligible evaporative cooling shown for the descending parcels in Figure 9. The changes in potential temperature for parcels initiated in the six cross-sections, plotted in Figure 10(b) and summarised in Table 2, show that, for the most part, the amount of latent cooling is small, usually less than 1 K. Assuming that the

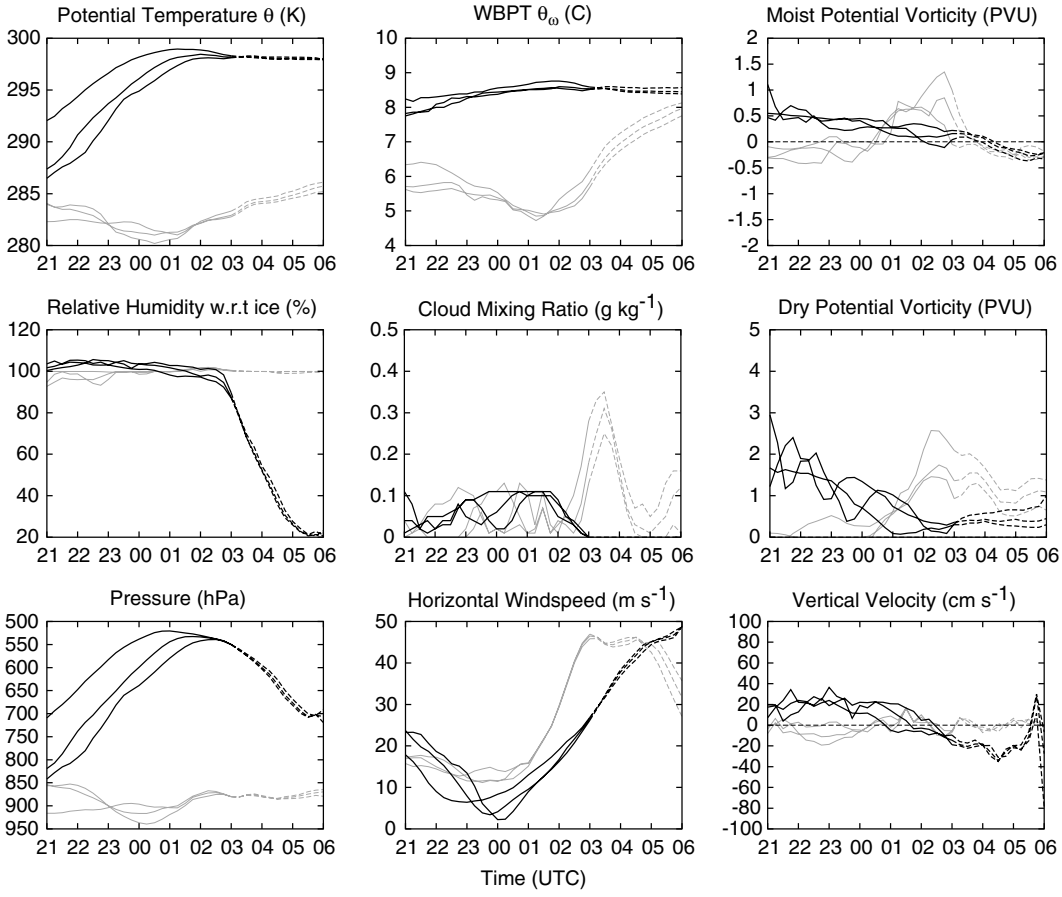

Figure 9. Trajectory diagnostics for the CJ and SJ2 parcels initiated at 0300 UTC on 3 January. Backward trajectories (solid lines) and forward trajectories (dashed lines) for CJ parcels initialised at cross-section D (D–D′) are in light grey and for SJ2 parcels initialised at cross-section B (B–B′) are in black. Time is in model hours (UTC).

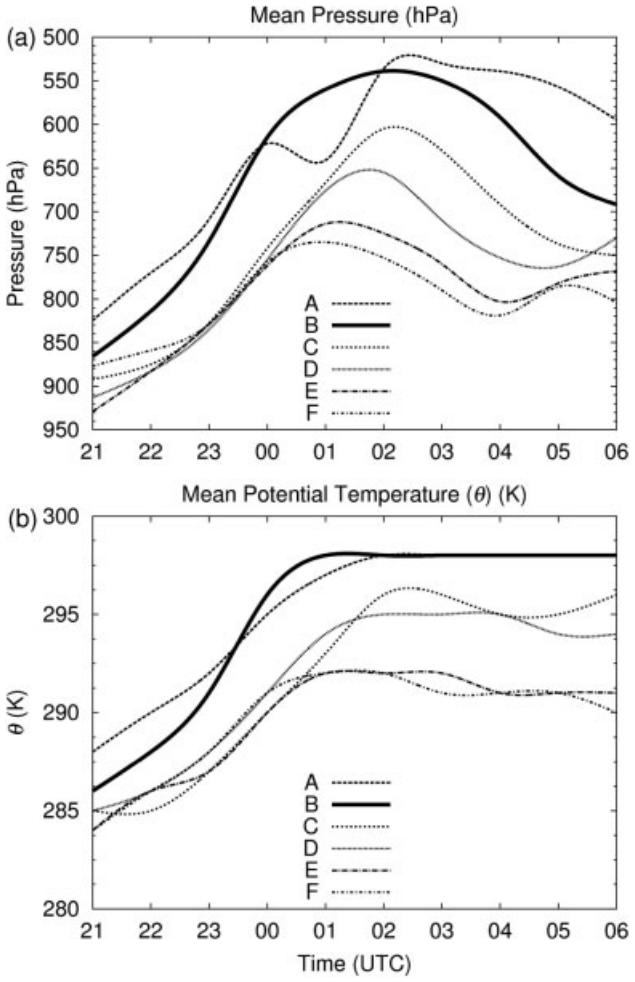

Figure 10. Mean properties of trajectory parcels initialised in the SJ2 core at cross-sections A (A–A′) to F (F–F′): (a) mean pressure (hPa), and (b) mean θ (K). Time is in model hours (UTC).

model is capable of properly representing the evaporative cooling, this would suggest that this was not an important mechanism for the SJ in this storm. However, there is evidence (not shown), of a decrease in potential temperature of up to 3 K for parcels initiated 50 hPa below the core of the SJ once the SJ had descended below 700 hPa. It appears that this is due partly to evaporation of cloud in the moist layer immediately beneath the SJ, perhaps due to mixing with the overlying dry air from the core of the SJ. Such mixing would also account for the decrease in θ_w seen in the last section (F) in Table 2, but it also means that some of the decrease in (dry bulb) potential temperature (θ) in section F would also be a direct consequence of mixing with the cooler air below rather than being entirely due to evaporation associated with the mixing.

We shall now clarify the location of a SJ parcel within the bent-back frontal zone as it first ascended and then descended. We focus again on the parcel showing the greatest vertical excursion, the diagnostics for which were plotted in Figure 9. Figure 11 shows the plan position of this SJ2 parcel with respect to the frontal zone at effectively hourly intervals during this cycle. The four panels in Figure 11 are actually for (a) 1900, (b) 2200, (c) 0100 and (d) 0400 UTC, but for each panel we have plotted the system-relative positions of the parcel at ± 1 h (open circles) as well as the position at the map time (solid black circles). Figure 11(a) shows the parcel at 1800, 1900 and 2000 UTC on 2 January just before it started to ascend, during which time it had an earth-relative speed of 19 m s^{-1} and was close to the lowest model layer, i.e. close to the relatively warm sea surface. Figure 11(b) shows it at 2100, 2200 and 2300 UTC, having risen to the 650 hPa level by 2200 UTC, with a wind speed of only 8 m s^{-1}. Figure 11(c) shows it at 0000, 0100 and 0200 UTC on 3 January, at the end of its main period of ascent; by 0100 UTC it had reached the 520 hPa level. Figure 11(d) shows the parcel at 0300, 0400 and 0500 UTC during its main period of descent and increasing speed within the evaporating cloud head; at 0400 UTC it was at 610 hPa and by 0500 UTC it had reached the 670 hPa level, with a speed of 45 m s^{-1}. It subsequently reached its lowest level (705 hPa) at 0530 UTC with a speed of 46 m s^{-1} (Figure 9 and Table 2). Throughout this 12 h cycle of ascent and descent, this and the other SJ parcels remained within the frontal zone. Their θ_w value of 8 to 8.5 °C from 2200 UTC onwards implies that they were situated somewhat towards the cold side of the frontal zone, but definitely within it. Initially, when they were close to the sea surface, the parcels were in a weak part of the frontal zone, actually the warm frontal zone ahead of where it became bent back (Figure 11(a)). They then rose within the frontal zone where the warm front became the BBF (Figures 11(b, c)). Finally, while they were descending and accelerating, they were within the weakening frontal zone; this is where the frontal fracture was most pronounced.

We have derived vertical cross-sections in the vicinity of the SJ parcels where they commenced their ascent (not shown). For the period up to 2300 UTC on 2 January, they were within the boundary layer. Here there was weak potential instability and negative moist PV. The parcels began their ascent at typically 10 cm s^{-1} as resolved by the model. It is not clear whether this initial ascent was in the form of slantwise ascent perhaps due to CSI or to shallow (<1 km deep) upright convection. Either way, this was followed, after 2300 UTC, by slantwise ascent as the parcels rose above the boundary layer and began to ascend more rapidly within the stable frontal zone. Figure 9 shows that the identified SJ parcels experienced no significant negative moist PV at this stage, nor indeed until after 0400 UTC. A similar picture has been found (not shown) for the other parcels for the trajectories initiated in the different cross-sections, with the exception of a small negative excursion for those from section E. It would appear, therefore, that, overall, CSI did not play a major role in the evolution of these parcels. This does not necessarily rule out a role for CSI at other times and places in this storm, but a thorough investigation of this is beyond the limited scope of this article. Unfortunately, we cannot altogether rule out the possibility that the model was failing to represent the small-scale processes adequately; however, it seems more likely that neither CSI nor evaporation were playing a major role in this case. This would indicate that these processes were of minor importance compared to the larger-scale dynamical processes in generating the rapid increase in wind during the descent of the SJ air and might explain the relative weakness of the SJ compared to that in the October 1987 storm, for which evaporation and CSI were believed to have played a more significant role.

In summary, at 0300 UTC, the model indicates the presence of an area of strong surface wind gusts that is distinct from that due to the CJ and is attributable to a SJ, referred to as SJ2. The sting jet SJ2 is in a region of strong descent at the evaporating tip of the cloud head and

Table 2. Summary of properties of trajectory parcels initialised in the SJ2 core at cross-sections A (A–A′) to F (F–F′). In each case the values given here relate to the parcel initiated in the jet core at each section which exhibited the greatest descent rather than to the mean of the three parcels, although the difference is not large. Pressure values are rounded to the nearest 5 hPa, θ to the nearest 1 K, θ_w to 0.1 K and RH to the nearest 5%.

Trajectory set at cross-section:	A	B	C	D	E	F
Values at minimum pressure (*P*min)						
Time (UTC) on 3 January	0245	0100	0200	0130	0115	0100
Pressure (hPa)	480	520	610	650	710	700
Wind speed ($m\,s^{-1}$)	15	8	14	15	14	16
θ (K)	296	296	296	295	292	292
θ_w (°C)	8.5	8.5	8.4	8.5	8.0	8.5
Relative humidity (%)	100	100	100	105	100	100
Values at maximum pressure (*P*max)						
Time (UTC) on 3 January	0600	0530	0600	0430	0400	0400
Pressure (hPa)	650	705	760	770	800	820
Wind speed ($m\,s^{-1}$)	40	46	47	47	45	44
θ (K)	296	296	296	296	292	290
θ_w (°C)	8.3	8.3	8.2	8.4	7.8	8.0
Relative humidity (%)	40	20	30	20	50	60
*Difference between values at P*max *and P*min						
Time (h)	3.25	4.50	4.00	3.00	2.75	3.00
Pressure (hPa)	170	185	150	120	90	120
Wind speed ($m\,s^{-1}$)	35	38	33	32	31	28
θ (K)	0	0	0	1	0	−2
θ_w (C)	−0.2	−0.2	−0.2	−0.1	−0.2	−0.5
Relative humidity (%)	−60	−80	−70	−85	−50	−40

it was formed from air that had remained within the frontal zone while undergoing a cycle of ascent and descent over a 12 h period. The main acceleration occurred during the final 4 h period of descent towards the footprint of strong surface winds. The remains of another SJ, referred to as SJ1, contributed to another part of the footprint of strong surface winds and is discussed in section 4.2.

4.2. *The evolving footprint of strong surface winds*

We conclude our analysis of the model storm by showing in Figure 12 the evolution of the footprint of strong surface wind gusts and the pattern of θ_w at 950 hPa (i.e. within 200 m of the surface) during the process of frontal fracture and seclusion. The hourly plots in Figure 12 are plotted in a frame of reference following the storm such that the low-pressure centre lies in the upper-central area of the plotting window. Frontal fracture can be seen to get under-way during the hours after 2000 UTC on 2 January (Figure 12(a)) and a warm seclusion begins to appear by 0400 UTC on 3 January (Figure 12(i)). A surface wind maximum due to the cold-conveyor-belt jet, CJ, forms on the cold side of the BBF at 0100 UTC and rapidly intensifies to $40\,m\,s^{-1}$, expanding in area as the BBF begins to curve around cyclonically. A discrete wind maximum of over $34\,m\,s^{-1}$ due to the SJ appeared on the warm side of the fracturing BBF 2 h earlier, at 2300 UTC; this area of strong winds, associated with a θ_w of 10±1 °C, intensifies to over $38\,m\,s^{-1}$ during the ensuing 4 h. By 0300 UTC, this is augmented by an area of equally strong winds just behind it (but still ahead of the CJ maximum); this is associated with a θ_w of 8.5±0.5 °C. The detailed analysis for 0300 UTC in section 4.1 shows that this new area is due to the SJ referred to as SJ2. The area of strong winds that developed earlier and is characterised by the higher values of θ_w, is due to SJ1; according to the analysis of the vertical structure in section 4.1, only the lower portion of SJ1 remained at 0300 UTC. By 0400 UTC all these areas of strong wind have merged as the CJ continues to wrap cyclonically around the southern flank of the storm. A detailed 3D analysis of the storm at 0700 UTC on 3 January (not shown) suggests that this was because the CJ was undercutting the SJ(s) at the later times. We shall focus our attention in this section on the evolution up to 0300 UTC while the surface manifestations of the CJ and SJs were still easily distinguishable from one another.

Some key parameters are tabulated in Table 3 at hourly intervals from 2100 to 0300 UTC. The features described in this table correspond to the lower edges of the cores of the SJ and CJ as seen close to the surface at 10 m height. The cores of strong winds close to the surface do not necessarily occur directly beneath the true cores of the jets responsible for them; they do seem to in the case of the SJ but, for the CJ, the associated wind maximum at the surface is sometimes slightly displaced so as to be beneath the northern edge of the true core aloft. For simplicity, we shall now refer to the sting jet simply as SJ; in fact we shall be referring to SJ1 throughout except at 0300 UTC when SJ2 began to dominate over SJ1. Table 3 shows that:

- Prior to 0100 UTC on 3 January surface gusts associated with the SJ are stronger than those due to the CJ. Once the CJ had developed, however, the CJ gave slightly stronger winds at the surface than the SJ and eventually it largely displaced the SJ. (We have not investigated the possibility that further SJs may again have had an effect at the surface at much later times.) A significant part of the maximum surface gust speed from the SJ is contributed by the overall system velocity, the direction of which (210°) is close to that of the SJ at later times.

Table 3 also shows that there are several ways in which the surface manifestations of the SJ could be distinguished from those of the CJ:

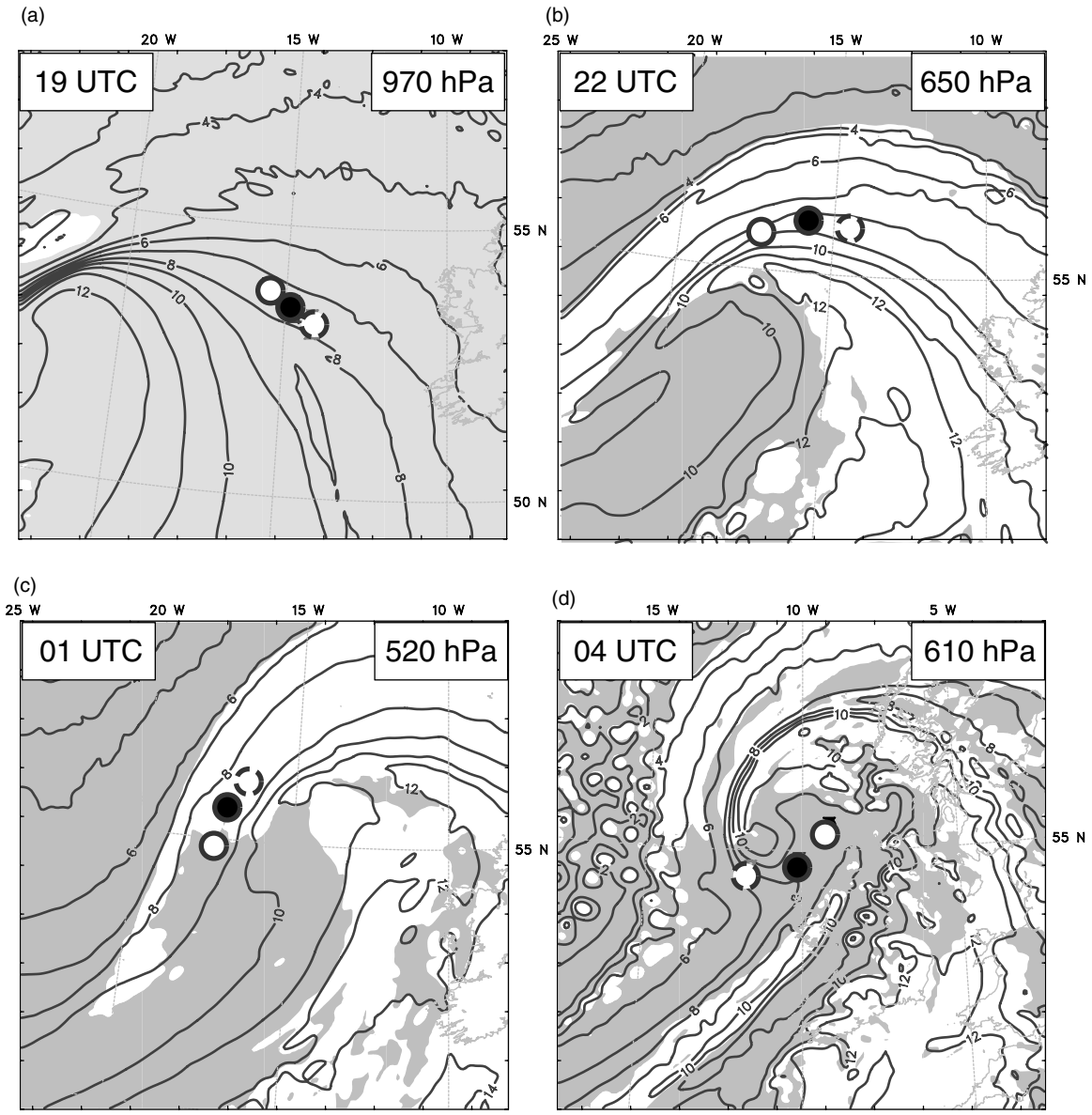

Figure 11. Plan positions of the SJ2 parcel that exhibited the greatest vertical excursion in Figure 9, plotted relative to the frontal zone and cloud head at 3 h intervals over a domain moving with the system: (a) 1900 UTC on 2 January on the 970 hPa pressure level, (b) 2200 UTC on 2 January at 650 hPa, (c) 0100 UTC on 3 January at 520 hPa, and (d) 0400 UTC on 3 January at 610 hPa. Cloud mixing ratio $>0.005\,\mathrm{g\,kg^{-1}}$ is shaded white. θ_w contours every 1 C. The parcel location at each time is indicated by a solid black circle; system-relative location of the parcel at -1 h is indicated by a dashed white circle and at $+1$ h by a solid white circle. Each frame is 1000×1000 km.

- The area of strong surface winds attributable to the SJ was accompanied by a θ_w that was significantly higher than that associated with the CJ, (although the difference decreased with time, especially at 0300 UTC when the strong surface winds were due to SJ2, the θ_w of which was lower than that of SJ1).
- The area of strong surface winds was drier in association with the SJ than with the CJ.
- The strong surface winds attributable to the SJ were substantially backed compared to those due to the CJ, by as much as 70° to 85°.
- The strong surface winds due to the SJ were in a much more divergent environment because of their occurrence within the region of frontal fracture (Figure 12).

We have added a dotted line to Figure 12(f, g, h) in to show where the descending air in the SJ has led, in the model, to the total dissipation of the boundary-layer stratocumulus in the region of strong low-level divergence. At 0100 UTC (Figure 12(f)), there is a close correspondence between the hole in the stratocumulus and the peak winds at the surface due to the SJ. By 0300 UTC, the hole in the cloud has been advected a little to one side of the area of strongest winds. A similar hole in the stratocumulus was observed in the satellite imagery in this case (e.g. beyond the tips of the cloud head filaments c and d in Figure 1(a)). Such holes are used by T. Hewson (personal communication) in his role as a chief forecaster in the Met Office as a means of identifying possible SJ situations.

We interpret the period 2300 to 0100 UTC as the 'early frontal fracture' stage, 0100 to 0300 UTC as the 'mature frontal fracture' and 0400 to 0700 UTC as the 'seclusion stage'. Recall that these are model times and that the model was 1 h slow. Therefore, at least for this phase of development for this simulated storm, the existence of a SJ that gives stronger surface winds than the CJ is confined to

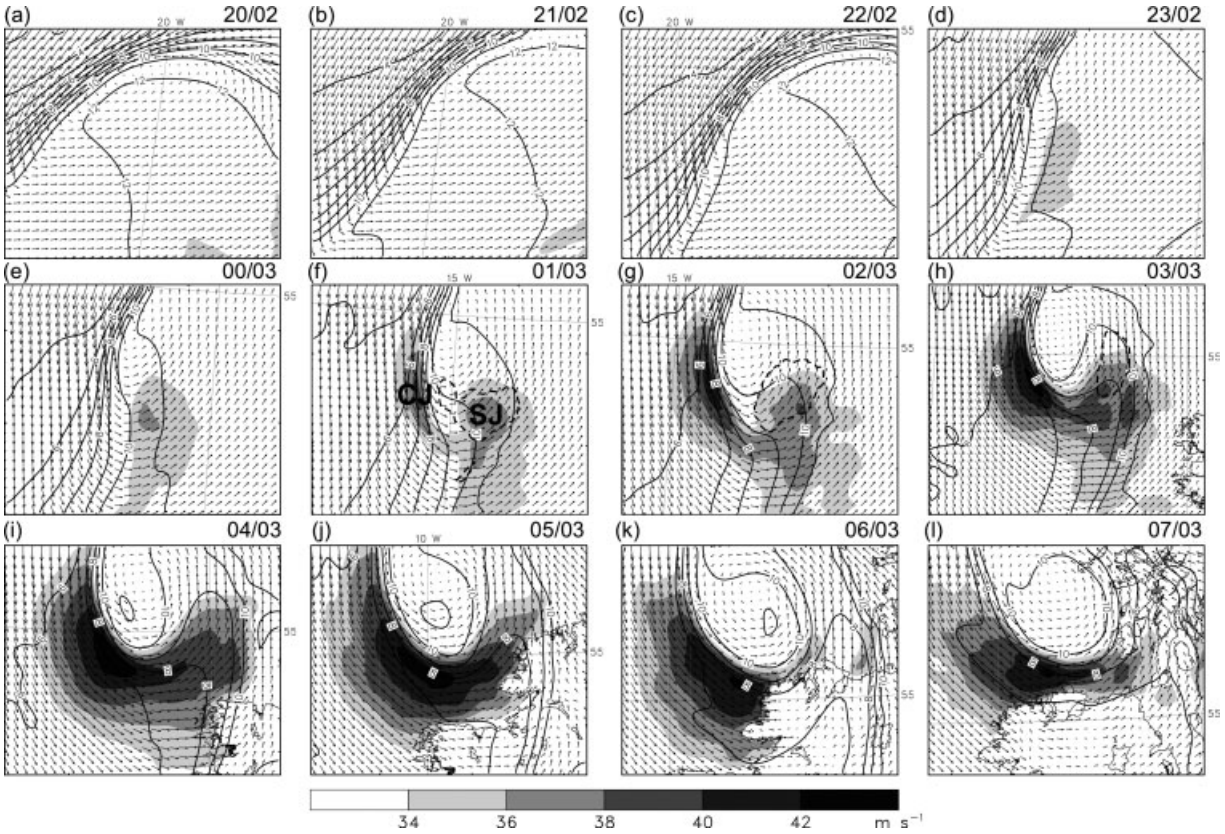

Figure 12. (a)–(l) The evolving footprint of strong surface winds plotted at 1 h intervals over a domain moving with the system, showing: 10 m wind gusts ($m\,s^{-1}$) shaded according to the key; θ_w at 950 hPa, contours every 1 °C; and system-relative flow vectors at 950 hPa. A system velocity of 17.9 $m\,s^{-1}$ from 210° is used throughout. The areas of strong surface winds attributed to the cold conveyor belt and sting jet, respectively, are labelled CJ and SJ in (f). The dashed line (in (f), (g) and (h) only and corresponding to the OLR 250 W m^{-2} contour) shows where the the descending SJ air has led to the total dissipation of the boundary-layer stratocumulus. The time (UTC)/day is given above the top right hand corner of each plot. Each plot is 300×250 km.

Table 3. Comparison of the properties of the lower edges of the CJ/**SJ** at 10 m above the surface. Figures for the **SJ** are in bold. Wind directions are estimated to the nearest 5°, and θ_w values to the nearest 0.5 °C. Divergence values are rounded to the nearest $5\times10^{-5}s^{-1}$.

Model time (UTC/day)	Maximum surface gust ($m\,s^{-1}$)	Wind direction at max. wind speed (° from north)	θ_w (°C)	Relative humidity (%)	Divergence ($10^{-5}s^{-1}$)
2100/02	30.2 / **30.8**	335 / **260**	6.5 / **11.0**	95 / **90**	0 / **0**
2200/02	31.5 / **32.9**	330 / **250**	6.5 / **11.0**	95 / **89**	0 / **5**
2300/02	33.6 / **34.1**	330 / **250**	6.5 / **10.5**	96 / **88**	0 / **5**
0000/03	35.2 / **36.8**	325 / **245**	7.0 / **10.0**	91 / **84**	5 / **10**
0100/03	38.5 / **37.8**	310 / **235**	7.0 / **10.0**	88 / **80**	10 / **15**
0200/03	45.1 / **38.1**	310 / **225**	8.0 / **9.5**	88 / **77**	10 / **30**
0300/03	46.3 / **42.1**	305 / **235**	8.0 / **8.5**	88 / **72**	5 / **25**

the 'early frontal fracture' stage (comparable to Stage II of the Shapiro–Keyser conceptual model; Shapiro and Keyser, 1990). The strength of the surface winds from both the SJ and the CJ continued to increase during the 'mature frontal fracture' stage, but with the surface effect of the CJ now dominating over that of the SJ. Even though the CJ was dominant at the later stage, the winds from the SJ were, however, still potentially damaging.

5. Discussion and conclusions

5.1. *Modelling issues*

This paper describes a successful simulation of the damaging windstorm that crossed northern Ireland and Scotland on 3 January 2012. In summary, we selected a GFS global model run which produced a storm that most nearly resembled the observed storm in terms of track and minimum SLP. This global run was used to initialise high-resolution nested runs of the WRF mesoscale model. We tried a variety of combinations of physical parametrisations and compared the outcomes with surface observations from Malin Head on the north coast of Ireland, where some of the strongest wind gusts (47 $m\,s^{-1}$) in this storm were recorded. We selected a configuration of the WRF that most closely reproduced those observations, particularly the wind velocities and cooling. Comparison with further observations suggested the chosen model run performed well in terms of track, minimum SLP and cloud-top morphology. The prediction of the strength of the surface winds was less accurate over land and so the analysis was focussed on structures occurring over the sea.

It was apparent from our 'ensemble' of different physics configurations (section 3) that the model near-surface fields were strongly dependent on the choice of microphysics, PBL and surface-layer parametrisation schemes. Although we have not discussed this in detail, analysis of the MYJ and MYNN runs (Table 1) produced quite different outcomes for the jets above and within the PBL (even though the resulting surface fields all appeared quite plausible). By comparing the model results with the Malin Head observations, we determined that the MYNN configuration produced results most nearly resembling the observed storm. The MYNN2 PBL module of this configuration, with its ability to predict greater vertical mixing than the MYJ scheme, was the likely key to this success.

Accurate prediction of the magnitude and areal extent of surface gusts is an important aspect of modelling severe extratropical cyclones for weather forecasting, climate change prediction and insurance risk assessment applications. The chosen MYNN run somewhat overpredicted wind gust strength in this case (Figure 3(a)) although 10 m mean winds were somewhat underpredicted. This may be because Malin Head, although on the coast, is still influenced significantly by the effect of the land. Whether adjustments to the empirically determined constant within the gust diagnostic (Schulz, 2008) would be justified remains to be seen. Overall, however, the resemblance of the model gust footprint to observations is encouraging, although the issue of the underestimation of surface winds over land remains to be resolved.

It is clear from this study and previous studies (e.g. Martinez-Alvarado *et al.*, 2010) that modern mesoscale models with different dynamical cores are capable of simulating SJ cyclones with reasonable realism. However, despite a variety of PBL modules being available in the WRF package, realistic depiction of the jets and boundary-layer structure remains problematic and poorly understood. The role of ice microphysics in producing evaporative cooling and strong winds and their depiction by the microphysics scheme is also an area requiring further research. It is difficult to assess with confidence the general performance and limitations of a particular model from just one case-study and analysis of further storms is needed, both in the context of operational forecasting and research applications.

The 5 km grid spacing used in the present study allows the resolution of fine-scale features in the simulation, yet this grid spacing is still insufficient to explicitly resolve small-scale convection and eddies above and within the PBL: a PBL parametrisation with the attendant uncertainties and assumptions is still required. Trajectory diagnostics from the present case suggest mixing is an important process in the evolution of both SJ and CJ, notably in how vertical momentum is transported to the surface in the form of gusts. Additionally, momentum may be transported by processes other than physical mixing, i.e. gravity waves (e.g. Businger, 1967), perhaps forced by the SJ at the PBL top. Resolution and depiction of such processes will require grid spacings of less (perhaps much less) than 1 km and/or significant improvements in PBL parametrisations.

We now summarise our understanding of the jets in the 3 January storm in the light of the MYNN simulation, whilst acknowledging the modelling caveats discussed above. This study was confined to the period of storm development shortly after commencement of frontal fracture up to the time of landfall of the region of strongest winds over northern Ireland. After this the mainland topography appears to have played a significant role in modifying the detailed structure of the storm and its surface winds, and we reserve examination of the later phase of the storm's life cycle for future research.

5.2. *The nature of the CJ and SJs*

These jets, especially SJs, are difficult to portray. The difficulty in portraying SJs arises because they not only have a short life time and small dimensions but also are sloping and strongly curved. Accordingly, in the present article, we adopt two new and complementary methods of portraying them. One method involves the derivation of a set of transverse cross-sections normal to the curved axes of the jets. The other method involves their depiction within surfaces of constant θ_w. This is particularly useful for the SJ for which θ_w is essentially conserved until it reaches low levels and starts to mix significantly with boundary-layer air.

The analysis of the mesoscale storm structure in section 4 showed that the model storm produced a principal CJ and two SJs as the BBF developed and started to wrap around the southwestern flank of the storm core. The CJ remained at low levels (below 850 hPa) in the cold air beneath the BBF, whilst the SJ was located within the frontal zone and sloped down from the middle troposphere to low levels. The CJ and SJs produced separate discrete surface gust maxima during the early stage of frontal fracture.

Distinct differences were identified in the properties of the regions of strong surface winds associated with the CJ and SJ. Surface conditions associated with the SJ were warmer and drier than those associated with the CJ. The associated surface winds were also substantially backed compared with those due to the CJ. These differences reflect the differences in the properties of the associated jets. Awareness of these differences may be helpful to forecasters in diagnosing model output and observations and seeking to differentiate between the effects of a CJ and a SJ.

The area of strong surface winds associated with the CJ was located just behind the BBF, whilst the area of strong surface winds associated with the SJs was located ahead of the BBF (and cloud-head hook) in the frontal fracture region of strong divergence, and hence widely spaced θ_w contours. The absence of significant vertical motion within the CJ is consistent with several previous studies, as summarised by Schultz (2001). The significant descent within the SJ is also in line with the earlier studies of SJs. The area of strong surface winds associated with the SJ was also accompanied by a localised tendency for the boundary-layer stratocumulus to dissipate, and this is already used by some forecasters as an indication of a possible SJ.

For a period of about 2 h, the maximum intensity of the SJ surface gust footprint was stronger than that of the CJ surface gust footprint. However, as the CJ wrapped around the southern flank of the storm core, the area of strong surface winds associated with the CJ became slightly more intense than the area associated with the SJ and eventually they merged. By 0700 UTC the effect of the SJ was mostly insulated from the surface by the CJ which was, by then, undercutting the SJ. Any remnant of the (surface expression) of the SJ would have passed over Malin Head prior to the time when surface gusts of 47 m s^{-1} were measured there. Thus another conclusion from this study, as in the study by Baker (2009), is that, just because a storm is identified as

having a SJ, it does not necessarily follow that the strongest surface winds will always be associated with the SJ. It may well be the case that the strongest winds in some extremely severe storms, such as the October 1987 storm, are due to the SJ (Clark *et al.*, 2005), but further research is required to determine the factors responsible for the exceptional strength of the SJ in such cases.

Schultz (2001), in his study of a cold conveyor belt, draws attention to the fact that parcel trajectories do not necessarily follow the system-relative streamlines within a cold conveyor belt because of the crudeness of the steady-state assumption. The same is true for a SJ, but this is not necessarily inconsistent with parcels following the axis of a SJ as its shape changes over time. An important issue that we have addressed is the extent to which the SJ can be considered to be a semi-Lagrangian feature in which air parcels can be assumed to travel along the entire axis of the jet as observed at an instant in time. This was found to be so to only a first approximation. By starting clusters of trajectories (forwards and backwards) at a given time from six widely different locations along the axis of the SJ, which extended over a distance of 200 km and a pressure range of 280 hPa (from the 520 hPa level down to 800 hPa), we found that only one of these clusters descended by as much as 185 hPa. The others descended by between 170 and 90 hPa. This is probably due, at least in part, to the short lifetime of a given SJ. In this study we identified two separate SJs, one of which was sufficiently discrete that we were able to determine its lifetime. It was detectable for only 5 h. Moreover, during much of this time it was relatively weak and possibly less extensive in the vertical. Thus it appears likely that the SJ typically dissipates or diminishes in intensity before a given parcel has time to travel along its entire length.

The model output shows that the air parcels that formed the SJ ascended slantwise, parallel to the sloping frontal zone, into the cloud head, before descending within the evaporating tip of the cloud head. Schultz and Sienkiewicz (2013) suggest that the vertical motion of the SJ air is due to frontogenetic forcing, with the descending part of the trajectory corresponding to the region of frontolysis where the spacing of the isentropes increases. They go on to suggest that the strong winds at low levels are due to this descent advecting strong winds from aloft down to the lower troposphere. However, our present study has shown that the wind speed of the SJ air just before it commenced its descent was quite low. The outstanding issue that still has to be resolved is what causes the SJ air to accelerate so strongly as it descends. Before they began their main ascent within the BBF, the SJ parcels emanated from within a boundary layer characterised by weak potential instability and negative moist PV. At this time they may have begun their ascent through very shallow upright convection (below 900 hPa) and/or through slantwise ascent due to CSI. However, the SJ parcels encountered no negative moist PV subsequently during their main transit through the cloud head.

Previous studies (e.g. Clark *et al.*, 2005) found that parcels experienced up to 3 K of evaporative cooling during their descent within the SJ, thereby supporting the hypothesis of a role for evaporation in the intensification of a SJ. This was not the case in the present study. Assuming that there are not gross deficiencies in the ability of the model to represent evaporative cooling, descending air parcels in the SJ appear to have undergone very little evaporative cooling: parcels were examined that were initiated over a wide range of locations along the jet axis but the evaporative cooling they experienced was seldom much in excess of 1 K. It is possible that this, together with the lack of CSI and the short lifetime of the SJs, may have been factors accounting for the present storm failing to give rise to surface winds that were as strong as those produced by the SJ in the October 1987 storm. The fact that the surface winds were nevertheless still damagingly strong can probably be ascribed to the primary forcing factors associated with the larger-scale dynamics but these have not been addressed in the present article.

Acknowledgements

We are indebted to Matthew Clark (Met Office, Exeter) who prepared Figure 4(a) with data supplied courtesy of and copyright the Met Office. Niall Dollard kindly supplied the data (courtesy of and copyright Met Éireann) used to prepare Figure 3. We thank Scott Bachmeier (CIMSS, University of Wisconsin-Madison) and Paul Blight for supplying satellite imagery. Geostationary satellite imagery is courtesy of and copyright Met Office and EUMETSAT.

We are grateful to Tim Hewson (Met Office/ ECMWF) and David Schultz (University of Manchester) for thought-provoking discussions, and the latter for providing a pre-print of Schultz and Sienkiewicz (2013). The paper has benefited from the comments of two anonymous referees.

References

Baker L. 2009. Sting jets in severe northern European wind storms. *Weather* **64**(6): 143–148.

Born K, Ludwig P, Pinto JG. 2012. Wind gust estimation for mid-European winter storms: towards a probabilistic view. *Tellus A* **64**: 17471.

Browning KA. 2004. The sting at the end of the tail: Damaging winds associated with extra-tropical cyclones. *Q. J. R. Meteorol. Soc.* **130**: 375–399.

Browning KA, Field M. 2004. Evidence from Meteosat imagery of the interaction of sting jets with the boundary layer. *Meteorol. Appl.* **11**: 277–289. DOI: 10.1017/S1350482704001379

Browning KA, Harrold TW. 1969. Air motion and precipitation growth in a wave depression. *Q. J. R. Meteorol. Soc.* **95**: 288–309.

Browning KA, Clough SA, Davitt CSA, Roberts NM, Hewson TD, Healey PGW. 1995. Observations of the mesoscale sub-structure in the cold air of a developing frontal cyclone. *Q. J. R. Meteorol. Soc.* **121**: 1229–1254.

Browning KA, Chapman D, Dixon RS. 2001. Stacked slantwise convective circulations. *Q. J. R. Meteorol. Soc.* **127**: 2513–2536.

Businger JA. 1967. Dissimilarity between vertical transfer of momentum and heat in the atmospheric boundary layer. *Phys. Fluids* **10**: S313. DOI: 10.1063/1.1762499

Carlson TN. 1980. Airflow through mid-latitude cyclones and the comma cloud pattern. *Mon. Weather Rev.* **108**: 1498–1509.

Clark PA, Browning KA, Wang C. 2005. The sting at the end of the tail: model diagnostics of fine-scale three-dimensional structure of the cloud head. *Q. J. R. Meteorol. Soc.* **131**: 2263–2292.

Gray SL, Martinez-Alvarado O, Baker LH, Clark PA. 2011. Conditional symmetric instability in sting-jet storms. *Q. J. R. Meteorol. Soc.* **37**: 1482–1500.

Grønås S. 1995. The seclusion intensification of the New Year's Day storm 1992. *Tellus A* **47**: 733–746.

Hong S-Y, Lim J-O. 2006. The WRF Single-Moment 6-class Microphysics Scheme (WSM6). *J. Korean Meteorol. Soc.* **42**: 129–151.

Martinez-Alvarado O, Weidle F, Gray SL. 2010. Sting jets in simulations of a real cyclone by two mesoscale models. *Mon. Weather Rev.* **138**: 4054–4075.

Martinez-Alvarado O, Gray SL, Catto JL, Clark PA. 2012. Sting jets

in intense winter North-Atlantic windstorms. *Environ. Res. Lett.* **7**: 024014. DOI: 10.1088/1748-9326/7/2/024014

Nakanishi M, Niino H. 2004. An improved Mellor–Yamada level-3 model with condensation physics: Its design and verification. *Boundary-Layer Meteorol.* **112**: 1–31.

Neiman PJ, Shapiro MA, Fedor LS. 1993. The life cycle of an extratropical marine cyclone. Part II: Mesoscale structure and diagnostics. *Mon. Weather Rev.* **121**: 2177–2199.

Parton GA, Vaughan G, Norton EG, Browning KA, Clark PA. 2009. Wind profiler observations of a sting jet. *Q. J. R. Meteorol. Soc.* **135**: 663–680.

Sanders F, Gyakum JR. 1980. Synoptic-dynamic climatology of the 'Bomb'. *Mon. Weather Rev.* **108**: 1589–1606.

Schulz J-P. 2008. 'Revision of the turbulent gust diagnostics in the COSMO model'. *COSMO Newsletter* **8**: 17–22. Available at http://www.cosmo-model.org

Schultz DM. 2001. Re-examining the cold conveyor belt. *Mon. Weather Rev.* **129**: 2205–2225.

Schultz DM, Sienkiewicz JM. 2013. Using frontogenesis to identify sting jets in extratropical cyclones. *Weather Forecasting* in press. DOI: 10.1175/WAF-D-12-00126.1

Shapiro MA, Keyser D. 1990. Fronts, jet streams and the tropopause. In *Extratropical Cyclones: The Erik Palmén Memorial Volume*. Newton CW, Holopainen EO. (eds) Amer. Meteorol. Soc: Boston, MA. 167–191.

Shutts GJ. 1990. Dynamical aspects of the October storm, 1987: A study of a successful fine-mesh simulation. *Q. J. R. Meteorol. Soc.* **116**: 1315–1347.

Skamarock WC, Klemp JB, Dudhia J, Gill DO, Barker DM, Duda MG, Huang X-Y, Wang W, Powers JG. 2008. '*A description of the Advanced Research WRF version 3*'. Technical Note NCAR/TN-475+STR. NCAR: Boulder, CO.

Stoelinga MT. 2009. '*A Users' Guide to RIP version 4.5: A program for visualizing mesoscale model output*'. Technical Note, University of Washington: Seattle, WA. http://www.mmm.ucar.edu/wrf/users/docs/ripug.htm

